REPORT DOCUMENTATION PAGE

Form Approved OMB No. 0704-0188

Public reporting burden for this collection of information is estimated to average 1 hour per response, including the time for reviewing instructions, searching existing data sources, gathering and maintaining the data needed, and completing and reviewing the collection of information. Send comments regarding this burden estimate or any other aspect of this collection of information, including suggestions for reducing the burden, to Department of Defense, Washington Headquarters Services, Directorate for Information Operations and Reports (0704-0188), 1215 Jefferson Davis Highway, Suite 1204, Arlington, VA 22202-4302. Respondents should be aware that notwithstanding any other provision of law, no person shall be subject to any penalty for failing to comply with a collection of information if it does not display a currently valid OMB control number.
PLEASE DO NOT RETURN YOUR FORM TO THE ABOVE ADDRESS.

1. REPORT DATE *(DD-MM-YYYY)* 15-03-2010	2. REPORT TYPE Final Report	3. DATES COVERED *(From – To)* 1 March 2007 - 11-Jun-10

4. TITLE AND SUBTITLE	5a. CONTRACT NUMBER
Frequency Extension of the Negative Index Materials (FENIM)	FA8655-07-1-3037
	5b. GRANT NUMBER
	5c. PROGRAM ELEMENT NUMBER

6. AUTHOR(S)	5d. PROJECT NUMBER
Professor Eleftherios N Economou	
	5d. TASK NUMBER
	5e. WORK UNIT NUMBER

7. PERFORMING ORGANIZATION NAME(S) AND ADDRESS(ES)	8. PERFORMING ORGANIZATION REPORT NUMBER
Foundation for Research and Technology, Hellas (FORTH) Vasilika Vouton, P.O. Box 1527 Heraklion, Crete 71110 Greece	N/A

9. SPONSORING/MONITORING AGENCY NAME(S) AND ADDRESS(ES)	10. SPONSOR/MONITOR'S ACRONYM(S)
EOARD Unit 4515 BOX 14 APO AE 09421	
	11. SPONSOR/MONITOR'S REPORT NUMBER(S) Grant 07-3037

12. DISTRIBUTION/AVAILABILITY STATEMENT

Approved for public release; distribution is unlimited.

13. SUPPLEMENTARY NOTES

14. ABSTRACT

This report results from a contract tasking Foundation for Research and Technology, Hellas (FORTH) as follows: The expected results include full understanding of the role of the periodicity on the negative index behavior. Exploitation of this understanding for optimization of Left Handed Materials (LHM) for different functionalities. (b) Negative Index Materials (NIM) operating in the THz regime and upwards. Determination of the frequency limits of the NIM behavior and understanding of the physical mechanism for these limits. Design, modeling, and, possible fabrication and characterization of negative index structures operating in the highest determined frequency limits. Deliverables: Reports on the results (a) and (b) mentioned above, at the end of the project, and interim reports documenting progress.

15. SUBJECT TERMS

EOARD, metamaterials, negative index materials, optical materials

16. SECURITY CLASSIFICATION OF:			17. LIMITATION OF ABSTRACT	18, NUMBER OF PAGES	19a. NAME OF RESPONSIBLE PERSON A. GAVRIELIDES
a. REPORT UNCLAS	b. ABSTRACT UNCLAS	c. THIS PAGE UNCLAS	UL	7	19b. TELEPHONE NUMBER *(Include area code)* +44 (0)1895 616205

Standard Form 298 (Rev. 8/98)
Prescribed by ANSI Std. Z39-18

"Frequency Extension of the Negative Index Materials" (FENIM)

Final report

In this report we briefly describe the work that has been done in the framework of FENIM since the interim reporting period.

The main issues that we were focused in this period are:

- Analysis and optimization of slab-pair-based designs for the achievement of high frequency negative permeability and negative index response.
- Investigation of connected metallic structures for achievement of negative index metamaterials that can be fabricated through direct laser writing.
- Superlensing based on anisotropic negative index metamaterials
- Investigation of Casimir forces in metamaterials – Demonstration (numerical) of repulsive Casimir forces in chiral metamaterials.

Below we briefly summarize our studies and the main results.

1. Analysis and optimization of slab-pair-based designs for the achievement of high frequency negative permeability and negative index metamaterials

While the first and most of the existing microwave negative index materials (NIMs) are systems made of split-ring resonators [1] (SRRs - see interim report) and continuous wires [2], in the high frequency (THz and optical) metamaterials the SRRs have been replaced by pairs of slabs (or stripes, or wires) - see Fig. 1(a). There, the resonant magnetic moment and the negative permeability are due to a resonant current mode with antiparallel currents in the two slabs of the pair, forming a loop-like current [3]. In most of the experimentally realized optical slab-pair&wire structures the slabs are as wide (at **H**-direction) as the corresponding unit cell side and are physically connected with the wires, leading to a design known as fishnet (see Fig. 1(d)) [4,5]. Fishnet design was able to give the highest in frequency NIMs up to now. (The main reason behind the replacement of SRR by the slab-pair for the high frequency metamaterials is its ability to exhibit negative permeability response for incidence normal to the plain of the pair; this makes possible the demonstration of the negative permeability response with just a monolayer of slab-pairs, greatly facilitating the practical realization.)

In this reporting period we studied the high-frequency magnetic response of systems based of pairs of slabs, which are scaled down from mm to sub-micron and nanometer scale. Our aim was to understand the response of those structures and to be able to optimize the structures as to achieve negative index materials of the highest possible operation frequency, with large operation bandwidth and acceptable losses. The structures that we have restricted our study are those shown in Fig. 1.

As a first step we examined numerically the wave propagation in those structures, determining their magnetic resonance frequency, the form of resonant permeability and the band-width of the negative permeability band. At a second step, using an effective resistor-inductor-capacitor (RLC) model, we analyzed and interpreted the numerical results and we used them to derive design rules for achievement of high frequency magnetic metamaterials and negative index materials of improved performance.
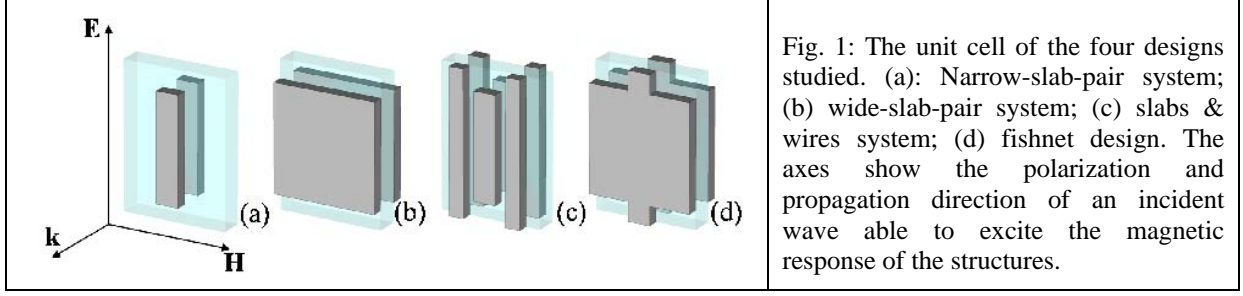
Fig. 1: The unit cell of the four designs studied. (a): Narrow-slab-pair system; (b) wide-slab-pair system; (c) slabs & wires system; (d) fishnet design. The axes show the polarization and propagation direction of an incident wave able to excite the magnetic response of the structures.

The results of our numerical study can be summarized as follows:

a) The magnetic resonance frequency, ω_m, (see Fig. 2a) of all the slab-pair-based structures follows the same behavior as the one reported earlier for SRR structures (see interim report): while in larger length-scales the magnetic resonance frequency scales inversely proportional to the lattice constant, at frequencies in the near IR towards optical regime this linear scaling breaks down, and the magnetic resonance frequency saturates to a constant value. This saturation value depends on the design and it is independent of the ohmic losses. Among our four designs fishnet was found to have the highest magnetic resonance saturation frequency, while all designs showed higher saturation values than U-shape SRRs of the same length-scale.

b) The relative band width ($\Delta\omega/\omega_m$) of the negative permeability regime (see Fig. 2b), while it remains constant for larger length scales (mm size) and smaller frequencies, in smaller scales (in the saturation regime of the magnetic resonance frequency) it decreases, tending ultimately to zero. This spectral width is very weakly dependent of the ohmic losses, showing that even in the absence of ohmic losses the negative µ spectral regime ultimately vanishes in smaller length-scale structures. We have to stress our unexpected finding that fishnet, which shows the highest magnetic resonance frequencies and generally considered as the superior design, shows the smallest bandwidth among our four designs.
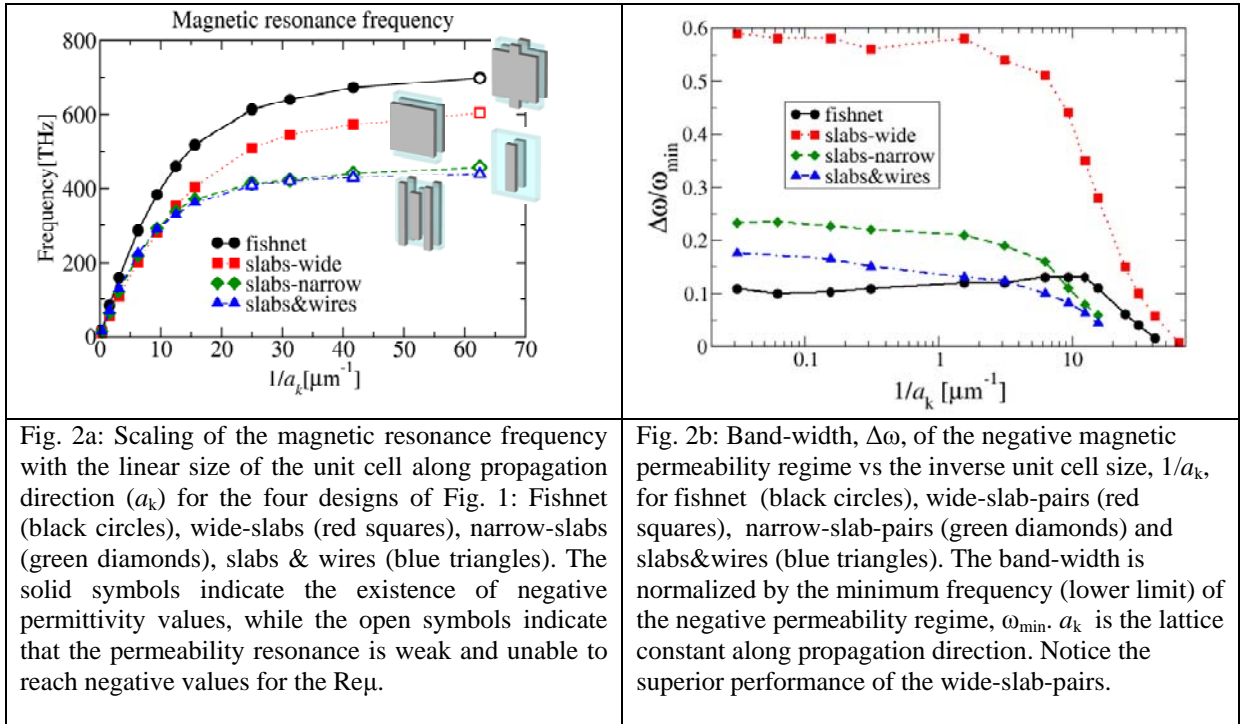

Fig. 2a: Scaling of the magnetic resonance frequency with the linear size of the unit cell along propagation direction (a_k) for the four designs of Fig. 1: Fishnet (black circles), wide-slabs (red squares), narrow-slabs (green diamonds), slabs & wires (blue triangles). The solid symbols indicate the existence of negative permittivity values, while the open symbols indicate that the permeability resonance is weak and unable to reach negative values for the Reµ.

Fig. 2b: Band-width, $\Delta\omega$, of the negative magnetic permeability regime vs the inverse unit cell size, $1/a_k$, for fishnet (black circles), wide-slab-pairs (red squares), narrow-slab-pairs (green diamonds) and slabs&wires (blue triangles). The band-width is normalized by the minimum frequency (lower limit) of the negative permeability regime, ω_{min}. a_k is the lattice constant along propagation direction. Notice the superior performance of the wide-slab-pairs.

c) The resonance of the magnetic permeability (see Fig. 3) becomes weaker and weaker as we move towards the nanoregime and ultimately ceases to reach negative values, as it has been observed earlier for SRR structures (see interim report).

d) The losses in the structures increase by reducing the length scale, approaching a saturation regime too.

To understand and reproduce the above mentioned results we used an RLC circuit model, which describes our artificial magnetic structures as RLC circuits driven by an external magnetic field. Using this model, one can calculate the current in the structures and through it the magnetic moment and the effective magnetic permeability.

The crucial point in analyzing the high frequency magnetic response of our structures is to take into account the high frequency response of the current carrying electrons in the metallic elements. This can be done by considering a Drude-type frequency dependent conductivity,

$$\sigma = i\varepsilon_0 \frac{\omega_p^2}{\omega^2 + i\gamma_m} \text{, leading to a total resistance } R_{tot} = \frac{1}{\sigma}\frac{l}{S} = (\frac{\gamma_m}{\varepsilon_0 \omega_p^2} - i\frac{\omega}{\varepsilon_0 \omega_p^2})\frac{l}{S} = R - i\omega L_e \text{.}$$

(where ω_p is the plasma frequency of the bulk metal, γ_m its colission frequency, l the length of the slab along the electric field direction, and S its (**k**-**H**) cross-section (see Fig. 1)).

The consideration of the frequency dependence in the conductivity results, besides the usual term R (representing the ohmic losses) in the total resistance, to an inductive resistance part, L_e, (electrons inductance), representing the inductance of the current-carrying electrons due to their kinetic energy. Using $R_{tot} = R - i\omega L_e$ in the Kirkhoff voltage rule for the RLC circuit representing the structure, one can see that the inductance L_e is added to the magnetic field inductance, L, resulting to a magnetic permeability form in a system of slab-pairs given by

$$\mu(\omega) = 1 - \frac{F'\omega^2}{\omega^2 - \omega_m^2 + i\omega\gamma'} \text{ with } \omega_m = \frac{1}{\sqrt{(L+L_e)C}} \text{ , } F' = F\frac{L}{L+L_e} \text{ , } \boxed{\gamma' = \frac{R}{L+L_e}}$$

(C is the structure capacitance and F is the volume fraction of the pair within the unit cell). Examining the scaling behavior of L, C, L_e and R, as the length scale of the structure is reduced, one can see that while the magnetic field inductance and the capacitance scale proportionally to the structure length scale (e.g. unit cell side), the electron inductance and the resisance scale inversely proportional, dominating thus the propagation at the nano-length-scales. This scaling behavior of L, C, L_e, R, combined with the above equations are able to reproduce all the features of the high frequency magnetic response of our structures.
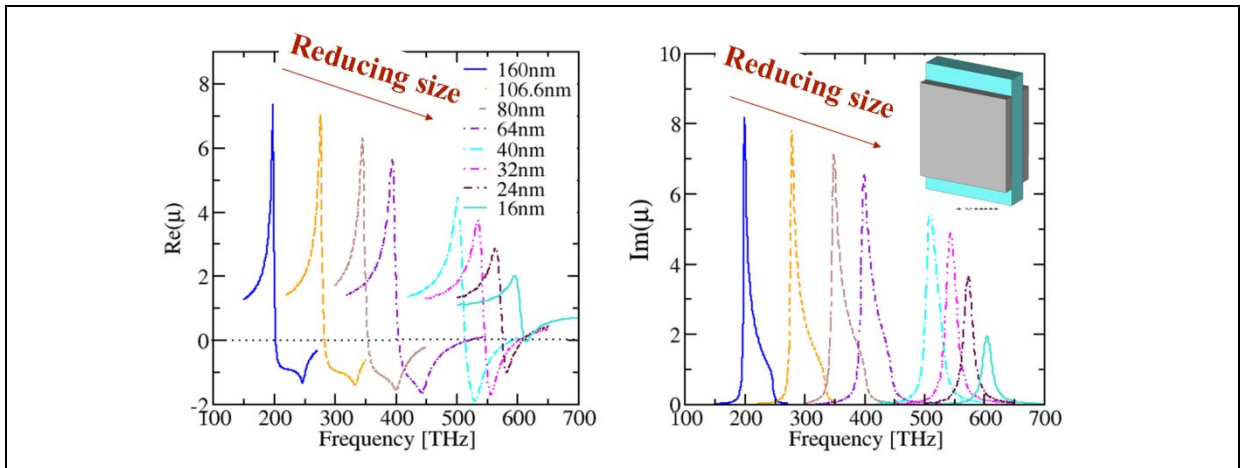

Fig. 3: Frequency dependence of the real (left panel) and the imaginary (right panel) part of the magnetic permeability of the wide slab-pair system for various length scales. The legends indicate the lattice constant along propagation direction for each specific system.
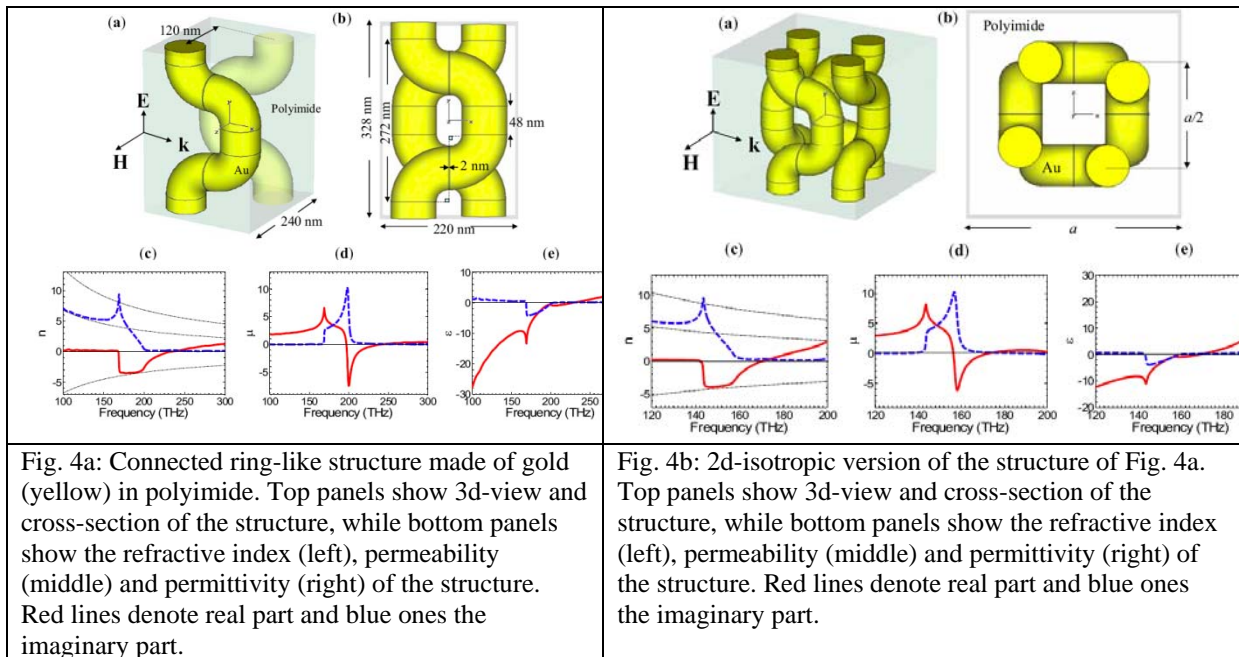
Structures optimization: Guided from the above formulas one can see that to achieve optimized high frequency metamaterial response one should pursue high magnetic resonance frequency, high factor F and low γ'. This leads to the requirement of small capacitance and small electrons inductance,

while small magnetic field inductance facilitates high magnetic resonance frequencies but leads to lower quality resonance and higher losses (and vice versa). In the case of slab-pairs the above conditions are translated to thick and wide slabs, thick separation layers, and metals of the highest possible plasma frequency and the lowest possible collission requency.

For detailed analysis and optimization rules see Related Publication [1].

2. Connected metamaterial structures for fabrication through direct laser writing

One of the challenges of today's research on high frequency metamaterials is the fabrication of such materials, since the current fabrication techniques are difficult, expensive, time consuming, and they have serious restrictions in the designs that they can implement (for example, e-beam lithography is able to produce planar structures while it is not easy to give 2d or 3d isotropic designs). Thus new techniques are required, able to cover the limitations of the current technologies. Such a promising technique seems to be a technique known as direct laser writing (DLR). DLR, although it is fast and easy to apply technique, it has the limitation that the only structures it can with physically connected metallic components; that's why it made crucial the design of new structures having connected metal patterns. Our attempts to design such structures led to the design of Fig. 4a, made of meandering metallic wires, which behave as rings perpendicularly to the external magnetic field direction and as continuous wires along the external electric field direction. This design was able to give negative index in the telecommunication wavelength of 1.5 μm with relatively low losses. One of the advantages of this design is that it can be easily extended to two-dimensions, giving a two-dimensional isotropic design as shown in Fig. 4b. The designs of Fig. 4a and 4b are under fabrication by the University of Karlsruhe.

Fig. 4a: Connected ring-like structure made of gold (yellow) in polyimide. Top panels show 3d-view and cross-section of the structure, while bottom panels show the refractive index (left), permeability (middle) and permittivity (right) of the structure. Red lines denote real part and blue ones the imaginary part.

Fig. 4b: 2d-isotropic version of the structure of Fig. 4a. Top panels show 3d-view and cross-section of the structure, while bottom panels show the refractive index (left), permeability (middle) and permittivity (right) of the structure. Red lines denote real part and blue ones the imaginary part.

3. Superlensing based on anisotropic left-handed metamaterials

Since most of today's negative index metamaterials in the optical regime are essentially anisotropic (since they are planar structures), it is crucial to examine if such kind of anisotropic metamaterials can lead to superlensing (i.e. focusing with resolution beyond the diffraction limit), as it has been shown for isotropic negative index materials. (Note that the superlensing capability of NIMs [6] constitutes the basis of most of the proposed potential applications of NIMs in the optical regime.)

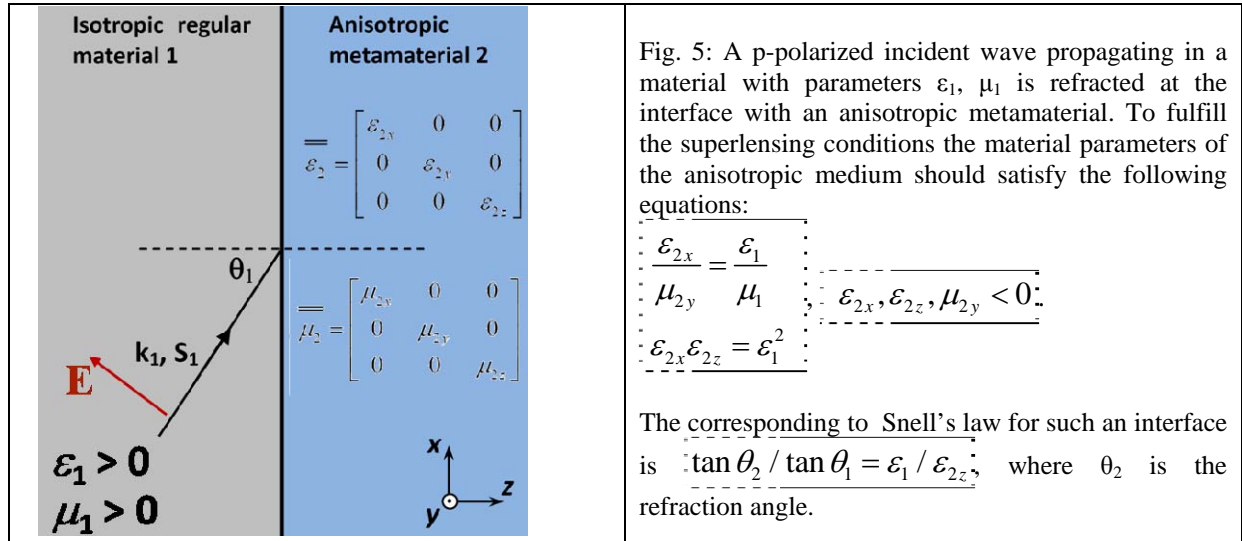Thus, we examined the possibility of achieving superlensing using anisotropic metamaterials of the form

$$\overline{\overline{\varepsilon_2}} = \begin{bmatrix} \varepsilon_{2x} & 0 & 0 \\ 0 & \varepsilon_{2y} & 0 \\ 0 & 0 & \varepsilon_{2z} \end{bmatrix}, \overline{\overline{\mu_2}} = \begin{bmatrix} \mu_{2x} & 0 & 0 \\ 0 & \mu_{2y} & 0 \\ 0 & 0 & \mu_{2z} \end{bmatrix}$$

Specifically, we examined if such materials can fulfill the conditions required for superlensing: (a) Omnidirectional total transmission for the propagating wave components emitted by a source object; (b) dispersionless surface plasmon modes for the evanescent components of an object.
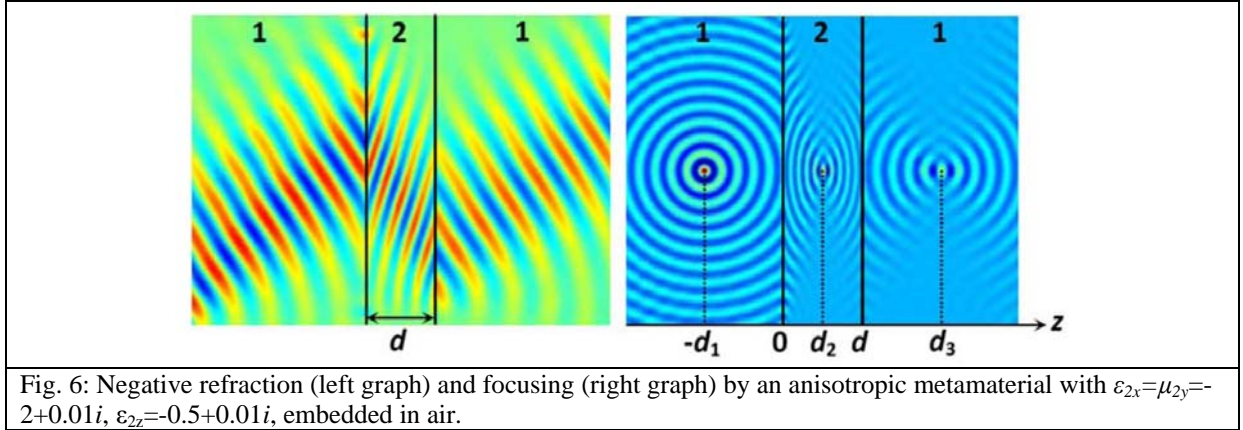
We found that indeed conditions (a) and (b) can be fulfilled in such anisotropic metamaterials. For that the required metamaterial parameters should obey the equations/conditions described in Fig. 5. These conditions are much easier to be fulfilled with structures made by planar technologies compared to the corresponding conditions for an isotropic negative index metamaterial ($\varepsilon_2 = -\varepsilon_1$, $\mu_2 = -\mu_1$).

The most important advantage though of such an anisotropic superlens is based on its proper lens formula, $d_{\text{Source}} + d_{\text{Image}} = (\varepsilon_{2x}/\varepsilon_1)d$, connecting the distance of source and image from the lens with the lens thickness, d (for an isotropic lens the corresponding formula is $d_{\text{Source}} + d_{\text{Image}} = d$) .

From this lens formula it can be concluded that a given source-image distance can be achieved with much thinner NIM slabs compared to the ones required in the isotropic lens case. This is extremely important in the optical regime, where reducing the lens thickness strongly reduces the losses, which are detrimental for the lens performance.

Fig. 5: A p-polarized incident wave propagating in a material with parameters ε_1, μ_1 is refracted at the interface with an anisotropic metamaterial. To fulfill the superlensing conditions the material parameters of the anisotropic medium should satisfy the following equations:

$$\frac{\varepsilon_{2x}}{\mu_{2y}} = \frac{\varepsilon_1}{\mu_1} \; ; \; \varepsilon_{2x}, \varepsilon_{2z}, \mu_{2y} < 0$$

$$\varepsilon_{2x}\varepsilon_{2z} = \varepsilon_1^2$$

The corresponding to Snell's law for such an interface is $\tan\theta_2/\tan\theta_1 = \varepsilon_1/\varepsilon_{2z}$; where θ_2 is the refraction angle.

The possibility of a material with parameters obeying the equations of Fig. 5 to lead to negative refraction and focusing is demonstrated in Fig. 6. Detailed analysis of our study concerning anisotropic superlensing can be found in the Related Publication [2].

Fig. 6: Negative refraction (left graph) and focusing (right graph) by an anisotropic metamaterial with $\varepsilon_{2x}=\mu_{2y}=-2+0.01i$, $\varepsilon_{2z}=-0.5+0.01i$, embedded in air.

4. Repulsive Casimir force in chiral metamaterials

Casimir force is the force between two material plates in close proximity. It has its origin in the electromagnetic energy vacuum fluctuations, and for regular materials it can be shown that it is always attractive. This attractive Casimir force can be detrimental, e.g., in micro- and nano-electro-mechanical systems where it can cause "stiction", i.e. collapse of the nearby metallic mechanical elements.

In this part of our research we examined the nature of Casimir forces between various types of planar metamaterial surfaces in close proximity. Our most important and novel idea was the employment of chiral metamaterials in connection with the Casimir effect. We found that the chirality reduces the attraction and that it may even lead to repulsion, if chirality is sufficiently strong We examined in detail the interaction energy between the two chiral metamaterial plates as their separation varies (see Fig. 7a) and we have shown that the sign of the force changes from attractive at large distances to repulsive at short distances passing through a stable equilibrium point of zero force, if the chirality strength exceeds a critical value. This critical value depends on the other parameters of the metamaterials involved.
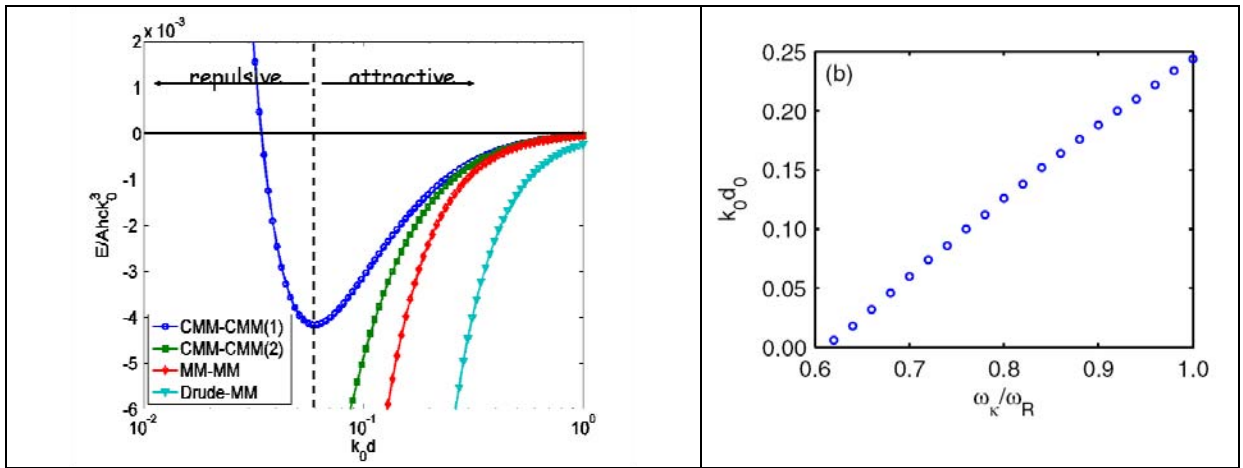

| Fig. 7a: Casimir interaction energy per unit area (E/A, normalized) as a function of a distance, d, of two chiral metamaterial plates, for different chirality strength, ω_k. The chirality parameter is proportional to ω_k. The wavenumber k_0 equals to the resonance frequency of the chirality parameter over the free space velocity of light, c. | Fig. 7b: The equilibrium distance, d_0, between the plates versus the chirality strength, ω_k. |

Moreover, we studied various realistic chiral structures in our effort to find out whether we can reach the required critical value of the chirality. For the calculation of Casimir force in the case of chiral metamaterials and the determination of the chirality strength of our designs (from reflection and transmission data) we had to extend the basic Casimir force theory [7] as well as the retrieval procedure in order to include chirality. We took into account that the constitutive relations are of the form $\mathbf{D}=\varepsilon_0\varepsilon\mathbf{E}+i\kappa\mathbf{H}/c_0$, $\mathbf{B}=\mu_0\mu\mathbf{H}-i\kappa\mathbf{E}/c_0$. ($\kappa$ is the chirality parameter, c_0 the vacuum speed of light and μ_0, ε_0 the permeability and permittivity of free space respectively) and, as a result, the TM and the TE components of the electromagnetic field are coupled together. Details of this study are discussed in our Related Publication [3].

Related publications

[1] R. S. Penciu, M. Kafesaki, Th. Koschny, E. N. Economou, and C. M. Soukoulis, "Magnetic response of nanoscale left-handed metamaterials", submitted to Phys. Rev. B.

[2] N. H. Shen, S. Foteinopoulou, M. Kafesaki, Th. Koschny, E. Ozbay, E. N. Economou, and C. M. Soukoulis, *Compact planar far-field superlens based on anisotropic left-handed metamaterials*, Phys. Rev. B **80**, pp. 115123-(1-9) (2009).

[3] R. Zhao, J. Zhou, Th. Koschny, E. N. Economou, and C. M. Soukoulis, « Repulsive Casimir Force in Chiral Metamaterials », Phys. Rev. Lett. **103**, 103602 (2009).

References

1. J. B. Pendry, A. Holden, D. Robbins, and W. Stewart, IEEE Trans. Microwave Theory Tech. **47**, 2075 (1999).

2. J. B. Pendry, A. T. Holden, W.J. Stewart and I. Youngs, Phys. Rev. Lett. **25**, 4773 (1996); J. B. Pendry, A. J. Holden, D. J. Robbins, and W. J. Stewart, J. Phys. Cond. Matt. **10**, 4785 (1998).

3. V. M. Shalaev, W. Cai, U.K. Chettiar, H.-K. Yuan, A.K. Sarychev, V.P. Drachev, and A.V. Kildishev, Opt. Lett. **30**, No.24, 3356 (2005);

4. S. Zhang, et al., Phys. Rev. Lett. **95**, 137404 (2005); S. Zhang, et al., Phys. Rev. Lett. **94**, 37402 (2005).

5. M. Kafesaki, I. Tsiapa, N. Katsarakis, Th. Koschny, C. M. Soukoulis and E. N. Economou, Phys. Rev. B **75**, 235114 (2007).

6. J. B. Pendry, Phys. Rev. Lett. **85**, 3966 (2000).

7. E.M. Lifshitz, Sov. Phys. JETP **2**, 73 (1956).